ELSEVIER

Polymer 43 (2002) 6569–6574

polymer

www.elsevier.com/locate/polymer

WAXD study of induced crystallization and orientation in poly(ethylene terephthalate) during biaxial elongation

Yann Marco*, Luc Chevalier, Mohend Chaouche

LMT-Cachan, ENS Cachan/CNRS-UMR 8535/Université Paris 6, 61 avenue du Président Wilson, 94235 Cachan Cedex, France

Received 15 April 2002; received in revised form 1 July 2002; accepted 15 July 2002

Abstract

This study presents an experimental investigation into the strain-induced crystalline microstructure, under biaxial elongation in poly(ethylene terephthalate) (PET), using wide angle X-ray diffraction (WAXD). We examined how the microstructure of a polymer subjected to a complex strain field evolves in terms of its crystalline ratio, its molecular orientation and the size of its crystallite. PET injection-molded specimens have been subjected to biaxial elongation tests, both equibiaxial and sequential, at different drawing speeds, draw ratios and temperatures above and close to T_g. The strain field was determined using a home-developed image correlation technique that has allowed us to determine all the strain components at each point of the specimen, even with a non-homogeneous strain field. To minimize the effect of quiescent crystallization, specimens are quickly heated with infrared and the temperature was regulated during the test. At the end of the deformation process, the specimens were quenched to room temperature. Their microstructures were later investigated, using both differential densimetry and WAXD with a synchrotron beam. Influences of strain rate, temperature and strain path sequence on the size of the crystallites and their orientation are evaluated. © 2002 Published by Elsevier Science Ltd.

Keywords: Poly(ethylene terephthalate); Biaxial; Crystallization

1. Introduction

Poly(ethylene terephthalate) (PET) is extensively used in a semi-crystalline state in industry to manufacture bottles, films, fibers, etc. The mechanical properties of the product are primarily a function of the crystalline texture, the crystalline volume fraction and its molecular orientation and extension. These parameters are not only strongly affected by the thermal history of the polymer but also by its deformation/flow during processing. Therefore, understanding the relationship between the deformation characteristics (strain, stress, geometry, etc.) and the induced microstructure (crystalline state, chain orientation and stretching) is essential in order to make quantitative predictions about the final properties of the product such as its mechanical and optical properties, its gas permeability, etc.

X-ray diffraction provides one of the most powerful techniques for characterizing the crystalline texture most accurately. Considerable work has been undertaken to investigate the effects of strain on the induced crystallization of PET close to its T_g using X-ray scattering. Ex situ [1–3] as well as in situ synchrotron experiments [4–6] has been reported. In these studies, the influence of several parameters has been considered, including the draw rate, the draw ratio and the temperature.

In the study presented here, the microstructure was analyzed ex situ, i.e. after both stretching and relaxation. In most of the experiments reported in the literature on strain-induced crystallization, the stretching tests are uniaxial. However, in a real industrial process, such as blow molding, the polymer is often subjected to a much more complex strain field than in simple uniaxial drawing. Due to the high anisotropy of the molecular chains in polymer, the type of deformation affects the microstructure crucially. The purpose of this study is to consider the effects of complex deformation on strain-induced crystallization and molecular orientation. Multiaxial deformations are actually very difficult to perform tidily and are quite rare. Here, 'real' biaxial tests are carried out using a triaxial test machine, developed by our laboratory in collaboration with the company Schenck AG (Darmstadt, Germany). In order to ensure a rapid and uniform heating of the specimens above the polymer's T_g, we used an infra-red heating apparatus. The local stress is not measured here, but the strain field is determined using an image correlation technique. In

* Corresponding author. Tel.: +33-1-47-40-22-42; fax: +33-1-47-40-22.
E-mail address: marco@lmt.ens-cachan.fr (Y. Marco).

0032-3861/02/$ - see front matter © 2002 Published by Elsevier Science Ltd.
PII: S0032-3861(02)00488-3

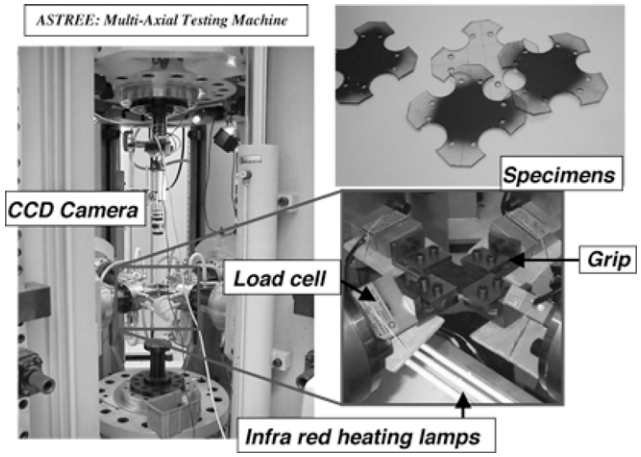

Fig. 1. Biaxial testing apparatus, triaxial testing machine Astree, biaxial specimens, IR heating apparatus.

Section 2, the mechanical experiments are described, including the stretching procedure, the strain field measurements, the heating system and the morphology measurement methods. In Section 3, we present and discuss the wide angle X-ray diffraction (WAXD) patterns, which permits to determine the crystallinity, the molecular orientation and the size of crystal lamellar as a function of local strain, temperature and strain rate.

2. Experiments

2.1. Biaxial tests

We briefly present here the biaxial set up (Fig. 1), which has been described in detail elsewhere [10]. The biaxial tests have been carried out on a triaxial testing machine named Astree (Fig. 1). Computer test control and data acquisition are performed by the object-oriented programming software, LabVIEW®. The material is a PET designed for blow-molding (PET 99 21 W EASTMAN). Our cross-shaped specimens (Fig. 1) are injection-molded, ensuring that our samples are initially amorphous. In order to determine the strain field, black paint and random whites spots are sprayed over one of the specimens' surface, and the evolution of the spray pattern with time can be followed by a CCD camera

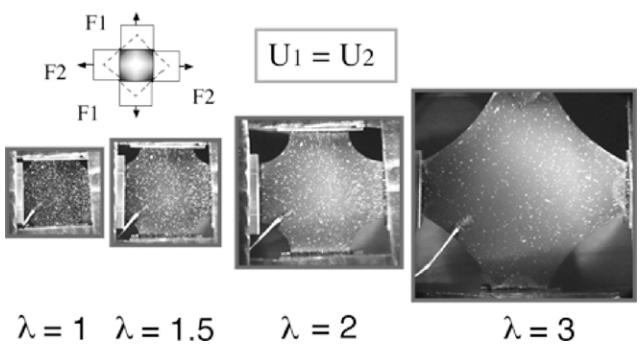

Fig. 2. Typical equibiaxial elongation test.

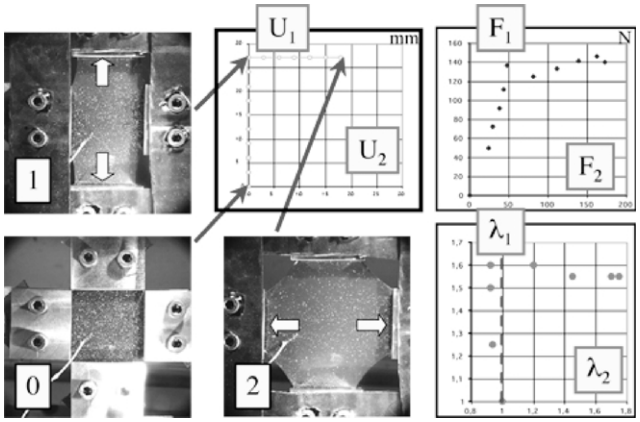

Fig. 3. Sequential biaxial loading, grip displacement U_1 and U_2, load F_1 and F_2 and elongations in the central region of specimens λ_1 and λ_2.

associated with an image analysis software (OPTIMAS). The evolution in time of the strain field is then determined using a home-developed cross correlation technique [8], implemented in Matlab™. The accuracy of the method is at least on the order of 2/100 pixels and the smallest displacement detectable is also on the order of 2/100 pixels. Fig. 4 shows typical results using this technique.

Like most polymers PET has low thermal conductivity. Heating techniques using convection or conduction not only require a long heating time, but also cause heterogeneity in the microstructure between the skin and the core of the material. An alternative is radiation heating with infrared waves. This method is commonly used in industry. The maximum variation of the temperature during a test is around $\pm 1°$. The specimen is heated on one side only, leaving the opposite side available for image acquisition with a CCD camera. Since the grips are not translucent to infrared light, only the testing zone of the specimen is heated and deformed which prevents the polymer from shrinking and slipping in the grips.

Two types of biaxial tension tests are carried out at different temperatures (90 and 100°C) and elongation speeds (8, 20 and 40 mm/s). The first one is an equibiaxial test in which the specimen is simultaneously stretched in the two perpendicular directions X_1 and X_2 (Fig. 2). The other type of biaxial tests is sequential biaxial: the specimen is stretched in the X_2 direction first and then in the X_1 direction (Fig. 3). Final draw ratios are the same for both types of tests.

Fig. 4 shows typical results obtained using Correli, our digital image correlation software. The displacement fields are clearly non-homogeneous in both biaxial tests. These results need to be compared with numerical simulations results, as has been done previously with natural rubber [9]. This study will be presented elsewhere.

2.2. Morphology analysis method

In a previous work [10], we showed that injected PET

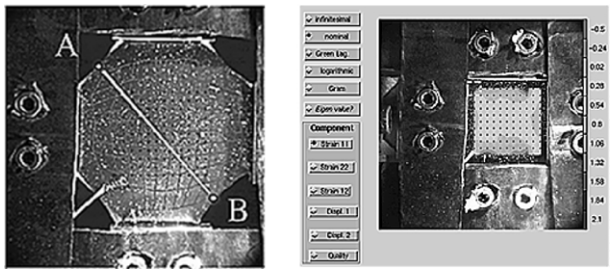

Fig. 4. Typical inter-correlation result for the equibiaxial test. (A) Typical displaced grid for equibiaxial testing. (B) ε_{11} nominal strain component.

specimens presents no initial orientation and only low initial crystallinity ($\approx 3\%$). We also verified also in that study that orientation (measured by IR dichroïsm) was homogeneous along the depth of the heated and stretched specimens and can thus be represented by only one variable f_c for the whole description of the specimen. This confirmed a posteriori the temperature homogeneity obtained by the infrared heating apparatus. Moreover, the study of thermal kinetics of PET confirmed that only very low thermal induced crystallinity could develop in the tests carried out here.

WAXD experiments are undertaken using a Synchrotron radiation source (beamline D43 of LURE (Orsay)). The specimens are scanned using a monochromated beam with a wavelength of 1.45 Å and a diameter of 0.5 mm. The sample to detector distance was 80 mm. Although no in situ measurements were carried out in this study, synchrotron radiation is still valuable because it makes it possible to measure thick specimens, which have seldom been studied. Moreover, it does not require any corrections due to X-ray mass attenuation for different thicknesses. The Debye–Scherrer patterns obtained are used to determine both the chain orientation and the crystallite geometry. The unit cell we chose is the one determined by Daubeny et al. [11].

The crystalline ratio can be inferred from the diffraction patterns, for example from the (010) crystal reflection peak area or the global comparison of amorphous and crystallized profiles. However, such methods have turned out to be less accurate than the density measurement technique, which we chose.

The ($\underline{1}05$) crystallographic plane, whose normal is close to the chain axis direction is studied. To determine the orientation in the whole volume, a study along the depth is necessary to take the out-of-plane rotation into account. As the scattering vector remained perpendicular to the specimen face, we could only get an evaluation of the orientation function f_c.

Assuming that benzene rings tend to lie down on the specimen plane and that chains remain mainly in the plane specimen, as noted elsewhere [12], this approximation seems to be coherent. We have also checked in a previous study [10] that orientation (measured by IR dichroïsm) was homogeneous along the depth of the heated and stretched specimens.

The Hermann crystalline orientation function f_c was

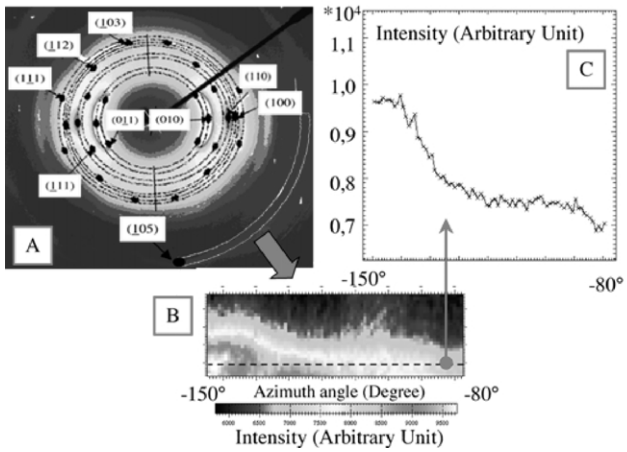

Fig. 5. Azimuthal scanning method. (A) WAXD pattern showing crystals reflections and the zone scanned. (B) Azimuthal scan presenting intensity versus 2θ and azimuth angles. (C) Profile obtained from a slice of the azimuthal scan for $2\theta_{(\underline{1}05)} = 39.6°$.

measured by azimuthal scanning of the ($\underline{1}05$) equatorial reflection (at $2\theta = 39.6°$) whose normal is close to the chain axis direction. Background intensity was measured at the tail ends and then subtracted. The average cosine square angle $\langle cos^2\phi_{\underline{1}05}\rangle$ (with ϕ the angle between the normal to ($\underline{1}05$) planes and the draw direction) was calculated from the corrected azimuthal intensities $I(\phi)$:

$$\langle \cos^2\phi_{\underline{1}05}\rangle = \frac{\int_0^{\pi/2} I(\phi)\sin\phi\cos^2\phi\,\mathrm{d}\phi}{\int_0^{\pi/2} I(\phi)\sin\phi\,\mathrm{d}\phi}$$

We assume that $\langle cos^2\phi_{\underline{1}05}\rangle$ is close to $\langle cos^2\phi_c\rangle$ the average cosine square of the angle between the c-chain axis and the draw direction. The crystalline orientation derives then from the Hermann orientation relationship:

$$f_c = \frac{3\langle \cos^2\phi_c\rangle - 1}{2}$$

Fig. 5 shows the method used to determine the local orientation of the chains. Fig. 5a represents a typical oriented WAXD pattern on which we have marked the crystallographic reflections. A half-quarter circular zone is scanned along the azimuth angle. Compared to some of the other reflections the intensity of the ($\underline{1}05$) reflection is too low to be seen on the WAXD pattern. Nevertheless, the integrated intensity azimuthal profile is large compared to the noise and can be used to calculate the orientation function. Fig. 5b represents the integrated intensity and we can see that the peak is right on the 2θ angle calculated from the Bragg relation ($2\theta = 39.57°$). Fig. 5c shows a slice of the integrated pattern for $2\theta = 39.57°$. This profile (when background contribution is subtracted) can be used to calculate $\langle cos^2\phi_{\underline{1}05}\rangle$ and then f_c. The azimuthal scans were performed thanks to the Fit2D software developed by the European Synchrotron Radiation Facility (ESRF).

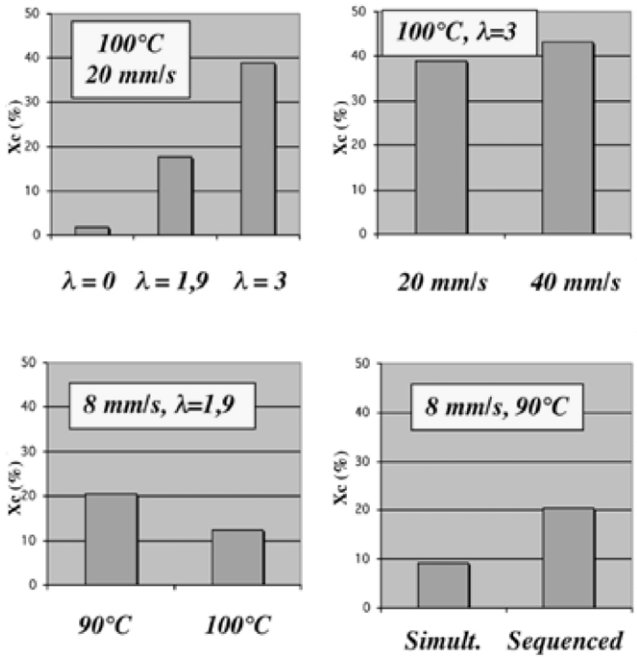

Fig. 6. Influence of elongation, strain rate, temperature and strain sequence on induced crystallization ratio.

The X-ray diffraction pattern also allows a quantitative study of the crystal lamellar morphology through a 2θ integration. The 2θ integrated profile of amorphous specimen is subtracted from the stretched ones. The profile is then deconvoluted using a curve-fitting program and the peaks are analyzed as PEARSON VII curves. The crystallographic planes investigated here are mainly ($\underline{1}05$) whose plane normal is close to the chain axis direction, (100) whose plane normal is close to the benzene ring normal, and (010). The reflections corresponding to these planes are pointed out in Fig. 5. Where the intensity of the reflection was too weak, we used the ($\underline{1}03$) reflection whose plane normal direction is close to that of ($\underline{1}05$).

The crystal size along the directions normal to these planes are then calculated using the Scherrer relation

$$L_{hkl} = \frac{\lambda}{\cos\theta_{hkl}\Delta\theta_{hkl}}$$

where $\Delta\theta_{hkl}$ is the angular width inferred from the deconvolution analysis. The crystallite size calculated seems to be large enough to avoid corrections due to artificial peak broadening [13].

In a recent paper [14] the best choice for the lower crystal lamellar size is discussed, and was determined as being either the crystal thickness (here normal to (010) plane) or the result the ($0\underline{1}1$) reflection. Yet, since the study using deconvolution remains difficult, especially in the case of oriented triclinic crystals such as PET, the difference between these two definitions is hardly noticeable. Moreover, given that the Scherrer relationship underestimates the lamellar size, a study along the (010) plane should give satisfactory average results.

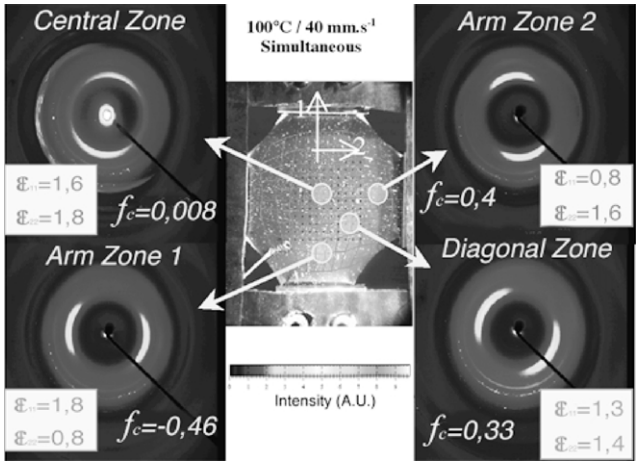

Fig. 7. Chain orientation at different points on the specimen.

3. Results and discussion

3.1. Crystallinity ratio

Fig. 6 shows crystallinity measurements undertaken on samples cut off from the central zone of specimens subjected to biaxial elongation tests. 'High strain' refers to an elongation ratio λ of about 3 and 'low strain' to an elongation ratio λ of about 2. As is well known in uniaxial elongation case, crystallization begins when a minimum strain has been reached. The critical elongation seems to be close to the one observed in the uniaxial case. Strain hardening and an increase of crystallinity appear during the second stage of elongation: typically above $\lambda = 2$. For the high strain test, the top-right chart in Fig. 6 shows the influence of strain rate: final crystallinity increases with speed. Of course this correlation saturates for very high-tension speeds since the ultimate crystallinity ratio is an upper bound. In the chart in the bottom-left, the effect of temperature is illustrated on two sequential biaxial tests. This result has also been observed on equibiaxial tests: as temperature increases, induced crystallinity decreases. The last chart (bottom-right) compares equibiaxial and sequential biaxial tests. This final observation has to be confirmed, since it is very difficult to obtain the same final strain field for both kinds of tests. It seems that initial orientation during the first stage of the sequential biaxial test helps to induce crystallization during the second stage. The sequence leads to a higher final crystallinity ratio.

3.2. Molecular orientation

Fig. 7 associates a macroscopic heterogeneous displacement and deformation field with the induced microstructure measured in different zones of the specimen during a simultaneous biaxial stretching test. As expected, the chains are strongly oriented along the draw direction in zones 1 and 2, where the strain is almost plane. In the central zone, where the strain is nearly equibiaxial, no preferential

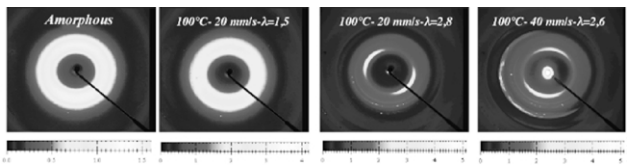

Fig. 8. Influence of strain ratio and rate on molecular orientation and size of crystallites.

orientation can be seen ($f_c \approx 0$). In the diagonal region, the chains are strongly oriented in the 45° direction, which is consistent with the fact that this corresponds to a shear strain zone. The orientations measured seem actually very close to the stress curves expected (linked to the conformation tensor) for this simultaneous test. So, as has been reported recently [7,15,16], for ex situ as well as in situ study, the chains orientation seems only slightly tilted through relaxation above a critical strain ratio, which is also confirmed by the little deviation (about 10°) of the equatorial reflections. This behavior could be explained by the strain-induced crystallization which could 'lock' the chain relaxation. This hypothesis is also supported by the high crystallinity ratio observed, although the latter might have been increased through relaxation. And indeed, if we assume that the retraction and reptation molecular times are close for uniaxial and biaxial cases, a comparison with a recent study by Mahendrasingam et al. [16] shows that an experiment undertaken in our conditions (strain rate and temperature) should lead to some crystallization occurring during the deformation, which could also confirm the lock-in of the chains conformation.

Figs. 8 and 9 show how experimental parameters (strain rate and ratio, temperature, strain sequence) can influence WAXD patterns. In these figures, we find again the same behavior that we have already discussed, i.e. there is a critical draw ratio and strain rate and temperature have opposite effects, which is also clearly observed in situ [17]. It should be noticed that for sequential tests, the molecular chains remain oriented along the first stretching direction as reported elsewhere for biaxial stretching of PET films [18], probably because the stretching along the second direction is not strong enough (low ratio) to break down the crystalline blocks and shift the orientation.

3.3. Crystal lamellar size

Two different regions of the specimens are studied, the central one where the elongation is equibiaxial and the ones

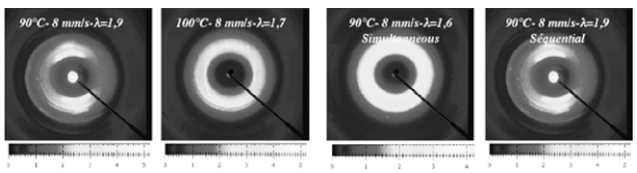

Fig. 9. Influence of temperature and type of sequence path on molecular orientation and size of crystallites.

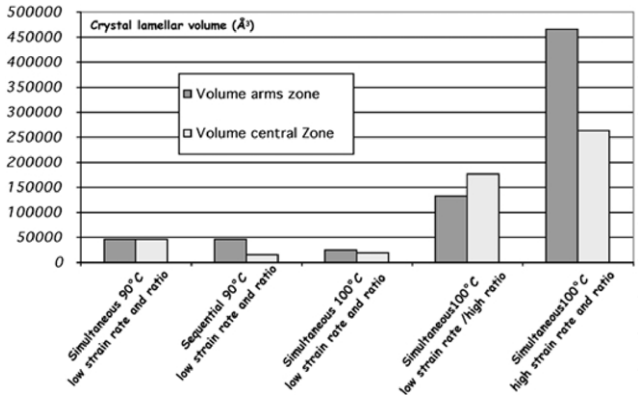

Fig. 10. Evolution of crystal lamellae volume in different experimental conditions.

near the grips where the elongations are close to those of a plane strain case (Fig. 7).

Knowing the size of the crystal along three independent directions allows us to gauge its volume. Fig. 10 presents the change in volume of the lamellar crystal in different experimental conditions. For low strains, the crystallites remain small at the two temperatures tested, whatever the strain rate. The opposite effects of temperature and strain rate can once again be observed. These tendencies are verified for both biaxial and plane strain zones. When the strain rate rises above a critical strain ratio, the volume of the crystallites increases very significantly. This is mainly caused by an important growth of lamellae along the chain axis as strain rate increases, and also by the fact that the length of the crystals along the (100) direction seems very sensitive to the draw ratio. It is worth noting that the growth of crystal lamellae along the chain axis is higher in 'plane-strain' zones than in the equibiaxial one. The lower length observed here is along the (010) direction. This 'thickness' is almost independent from the draw ratio, and the strain rate. The values for both kinds of zones are close and no influence of strain type can be seen. A possible explanation for these weak dependencies could be that an equilibrium has been reached, depending mainly from the stretching temperature.

If we compare the volume of the crystals to the crystallinity ratio measured it is possible to evaluate the average number of crystals per unit volume [3]. This shows the importance of the type of strain and history experimented by the material. For example, sequential tests lead to smaller but more numerous crystals, and there are even more of them in the equibiaxial strain zone. This illustrates the crumbling of the crystal blocks generated by the second stretching even if, as noted previously, the draw ratio was too low to change the former orientation. For high strain ratios, one can see that a higher strain rate generates bigger but fewer crystals, which differs from the in situ observations [16] where the half-width of the crystalline reflection seemed to remain essentially unchanged during the crystallization process. This could be explained by a

higher orientation during the stretching phase and more amorphous material converted into crystal during the relaxation [15].

4. Conclusions

During our study, we have developed and used a set of multiaxial experimental tools. Biaxial elongation experiments have been undertaken using a triaxial testing machine. To ensure a homogeneous and rapid heating of the polymer, we used an infrared heating apparatus. We determined the strain field with an image correlation technique. Different complex paths of biaxial stretching are possible: equibiaxial and sequential biaxial elongation tests have been presented here. Morphology measurements on biaxially stretched samples have been presented in terms of crystallinity, chain orientation and the size of the crystallites. It is worth noting that the microstructure induced in our biaxial tests is not actually an accurate representation of the one induced by the industrial blowing process. Along the thickness of a bottle, the microstructure is heterogeneous in terms of crystallinity and orientation [19], while our experiments lead to a homogeneous microstructure along the specimen's thickness. Some more experiments are to be carried out in order to confirm the tendencies highlighted here, and quenching protocols should be used in order to study the germination and growth of the crystals.

In order to identify the mechanical behavior under such complex thermo-mechanical solicitations, we are currently undertaking numerical simulations to be compared with experimental results. In a first study, molecular models are implemented [20–22] but more realistic models [23,24] are to be used. These models should, on the one hand take into account the strain induced crystallization and on the other hand, be representative of the material's behavior under a complex strain field.

Acknowledgments

To EASTMANN for providing us with the PET, to G. Régnier who allowed their injection and to J. Doucet for his help in the X-ray diffraction experiments. A special thanks to Pierre and Laura for english rewriting.

References

[1] Casey M. Polymer 1977;18:1219–26.
[2] Cakmak M, Spruiell JE, White JL, Lin JS. Polym Engng Sci 1987; 27(2):893–905.
[3] Vigny M, Tassin JF, Gibaud A, Lorentz G. Polym Engng Sci 1998;37: 1785–94.
[4] Mahendrasingam A, Martin C, Fuller W, Blundell DJ, MacKerron DH, Oldman J, Harvie JL, Riekel RC, Engström P. Polymer 1999;40: 5553–65.
[5] Pople JA, Mitchell GR, Sutton SJ, Vaughan AS, Chai CK. Polymer 1999;40:2769–77.
[6] Mahendrasingam A, Martin C, Fuller W, Blundell DJ, Oldman RJ, MacKerron DH, Harvie JL, Riekel RC. Polymer 2000;41:1217–21.
[7] Gorlier E, Haudin JM, Billon N. Polymer 2001;42:9541–9.
[8] Chevalier L, Calloch S, Hild F, Marco Y. Eur J Mech A/Solids 2001; 20:169–87.
[9] Chevalier L, Marco Y. Polym Engng Sci 2002;42(2).
[10] Marco Y, Chevalier L, Régnier G, Poitou A. Macromol Symp, Spec Issue FICOP 2001, 2002; in press.
[11] Daubeny RP, Bunn CW, Brown CJ. Proc R Soc Lond 1954;A(226): 531–42.
[12] Göshel U, Deutscher K, Abetz V. Polymer 1996;37:1.
[13] Guinier A. Théorie et technique de la radiocristallographie. Dunod 1956;463–89.
[14] Wang ZG, Hsiao BS, Liu BX, Yeh F, Sauer BB, Chang H, Schultz JM. Polymer 2000;41:1791–7.
[15] Matthews RG, Ajji A, Dumoulin MM, Prud'homme RE. Polymer 2000;41:7139–45.
[16] Mahendrasingam A, Blundell DJ, Martin C, Fuller W, MacKerron DH, Harvie JL, Oldman RJ, Riekel RC. Polymer 2000;41:7803–14.
[17] Blundell DJ, Mahendrasingam A, Martin C, Fuller W, MacKerron DH, Harvie JL, Oldman RJ, Riekel C. Polymer 2000;41:7793–802.
[18] Vigny M, Tassin JF, Lorentz G. Polymer 1999;40:397–406.
[19] Everall N, MacKerron D, Winter D. Polymer 2002;43:4217–23.
[20] Doi M, Edwards SF. J Chem Soc Faraday Trans II 1975;74: 1789–818.
[21] Doufas AK, Dairanieh IS, McHugh AJ. J Rheol 1999;43(1):85.
[22] Poitou A, Ammar A. C R Acad Sci, Paris 2001;t329(IIb):5.
[23] Boyce MC, Arruda EM. Polym Engng Sci 1990;30:1288.
[24] Buckley CP, Jones DC. Polymer 1995;36:3301.